

Magnetocrystalline anisotropy and dynamic spin reorientation of half-doped $Nd_{0.5}Pr_{0.5}FeO_3$ single crystal

Haotian Zhai(翟浩天), Tian Gao(高湉), Xu Zheng(郑旭), Jiali Li(李佳丽), Bin Chen(陈斌), Hongliang Dong(董洪亮), Zhiqiang Chen(陈志强), Gang Zhao(赵钢), Shixun Cao(曹世勋), Chuanbing Cai(蔡传兵), and Vyacheslav V. Marchenkov

Citation: Chin. Phys. B, 2021, 30 (**7**): 077502. DOI: 10.1088/1674-1056/ac0786
Journal homepage: http://cpb.iphy.ac.cn; http://iopscience.iop.org/cpb

What follows is a list of articles you may be interested in

Thickness-dependent magnetic anisotropy in obliquely deposited Fe(001)/Pd thin film bilayers probed by VNA-FMR

Qeemat Gul, Wei He(何为), Yan Li(李岩), Rui Sun(孙瑞), Na Li(李娜), Xu Yang(杨旭), Yang Li(李阳), Zi-Zhao Gong(弓子召), Zong-Kai Xie(谢宗凯), Xiang-Qun Zhang(张向群), Zhao-Hua Cheng(成昭华)
Chin. Phys. B, 2019, 28 (**7**): 077502. DOI: 10.1088/1674-1056/28/7/077502

Influence of additives on the magnetic damping constant of CoIr soft magnetic thin films with negative magnetocrystalline anisotropy

Tianyong Ma(马天勇), Zhi Luo(罗智), Zhiwei Li(李志伟), Liang Qiao(乔亮), Tao Wang(王涛), Fashen Li(李发伸)
Chin. Phys. B, 2019, 28 (**5**): 057505. DOI: 10.1088/1674-1056/28/5/057505

Mn-based permanent magnets

Jinbo Yang(杨金波), Wenyun Yang(杨文云), Zhuyin Shao(邵珠印), Dong Liang(梁栋), Hui Zhao(赵辉), Yuanhua Xia(夏元华), Yunbo Yang(杨云波)
Chin. Phys. B, 2018, 27 (**11**): 117503. DOI: 10.1088/1674-1056/27/11/117503

Negative dependence of surface magnetocrystalline anisotropy energy on film thickness in $Co_{33}Fe_{67}$ alloy

De-Lai Wang(王得来), Ming-Qi Cui(崔明启), Dong-Liang Yang(杨栋亮), Jun-Cai Dong(董俊才), Wei Xu(徐伟)
Chin. Phys. B, 2016, 25 (**10**): 107501. DOI: 10.1088/1674-1056/25/10/107501

Manipulating magnetic anisotropies of Co/MgO(001) ultrathin films via oblique deposition

Syed Sheraz Ahmad, Wei He(何为), Jin Tang(汤进), Yong Sheng Zhang(张永圣), Bo Hu(胡泊), Jun Ye(叶军), Qeemat Gul, Xiang-Qun Zhang(张向群), Zhao-Hua Cheng(成昭华)
Chin. Phys. B, 2016, 25 (**9**): 097501. DOI: 10.1088/1674-1056/25/9/097501

Magnetocrystalline anisotropy and dynamic spin reorientation of half-doped $Nd_{0.5}Pr_{0.5}FeO_3$ single crystal*

Haotian Zhai(翟浩天)[1], Tian Gao(高湉)[1,2,3,†], Xu Zheng(郑旭)[1], Jiali Li(李佳丽)[1], Bin Chen(陈斌)[2], Hongliang Dong(董洪亮)[2], Zhiqiang Chen(陈志强)[2], Gang Zhao(赵钢)[3], Shixun Cao(曹世勋)[3,‡], Chuanbing Cai(蔡传兵)[3], and Vyacheslav V. Marchenkov[4,5]

[1] *Department of Physics, Shanghai University of Electric Power, Shanghai* 200090, *China*
[2] *Center for High Pressure Science and Technology Advanced Research, Shanghai* 201203, *China*
[3] *Shanghai Key Laboratory of High Temperature Superconductors, Shanghai University, Shanghai* 200444, *China*
[4] *M. N. Mikheev Institute of Metal Physics, Ekaterinburg* 620108, *Russia*
[5] *Ural Federal University, Ekaterinburg* 620002, *Russia*

(Received 12 March 2021; revised manuscript received 6 April 2021; accepted manuscript online 3 June 2021)

The single crystals of $Nd_{0.5}Pr_{0.5}FeO_3$ were successfully grown by optical floating zone method. Room temperature x-ray diffraction and Laue photograph declared the homogeneity and high quality of the crystal. The significant magnetic anisotropy and multiple magnetic transitions illustrate the complex magnetic structure. At high temperatures ($T > 66$ K), it shows the typical characteristics of $\Gamma_4(G_x, A_y, F_z)$ state. With the decrease of the temperature, it undergoes a first-order spin reorientation transition from $\Gamma_4(G_x, A_y, F_z)$ to $\Gamma_2(F_x, C_y, G_z)$ state in the temperature window of 45–66 K under an applied magnetic field of 0.01 T. As the temperature drops to $\sim$ 17 K, a new magnetic interaction mechanism works, which results in a further enhancement of magnetization. The T–H phase diagram of $Nd_{0.5}Pr_{0.5}FeO_3$ single crystal was finally constructed.

Keywords: rare earth orthoferrite, magnetocrystalline anisotropy, magnetic ordering, magnetic hysteresis

PACS: 75.47.Lx, 75.30.Gw, 75.60.Ej, 61.50.–f **DOI:** 10.1088/1674-1056/ac0786

1. Introduction

In recent years, $RFeO_3$ (R means rare-earth elements) family has regained attention owing to its rich physical content and the fascinating potential applications, such as precession excitation induced by terahertz pluses, ambient multiferroics, laser-induced ultrafast spin reversal, ultrafast photomagnetic excitation, etc.[1–5] $RFeO_3$ ferrites usually crystallize in a distorted perovskite structure and contain two sets of magnetic sublattices, R^{3+} and Fe^{3+} ions. Three types of magnetic interactions are identified in this kind of rare-earth orthoferrites, Fe^{3+}–Fe^{3+}, R^{3+}–R^{3+}, and Fe^{3+}–R^{3+},[6,7] which make the magnetic behaviors complex and interesting. The magnetic moment of Fe^{3+} mainly comes from the unpaired electrons on the 3d shell. The antiferromagnetic (AFM) coupling of the neighboring Fe^{3+} ions is generated by the Fe–O–Fe super-exchange interaction.[8] However, the canted FeO_6 octahedra could induce a weak ferromagnetic (FM) moment due to the so-called antisymmetric Dzyaloshinskii–Moriya (DM) interactions.[9,10] On cooling, $RFeO_3$ may undergo two spin reorientation (SR) transitions originated from R–R and R–Fe interactions.[11] $PrFeO_3$ and $NdFeO_3$ come into a $\Gamma_2(F_x, C_y, G_z)$ phase from $\Gamma_4(G_x, A_y, F_z)$ phase in the temperature ranges of 6.5–10 K and 107–170 K, respectively.[12,13] Here, F means the weak FM moment because of the canted AFM ordering due to DM interactions, A, C and G mean the AFM orderings of A-, C- and G-type, respectively. That is, the resultant FM vector points along the c-direction of the crystal in Γ_4 state, and the a-direction in Γ_2 state. The strong interaction between the 3d outer electrons of Fe^{3+} and 4f electrons of R^{3+} is the main source for the magnetic configuration and magnetic phase transitions. However, the interaction mechanisms of Fe–Fe, R–R and R–Fe are unclear till now.

Researchers have tried many kinds of physical fields (such as optical pulse, temperature, magnetic field, etc) to regulate the SR of $RFeO_3$ ferrites,[14] so that they can have a deeper understanding to the behavior of 4f and/or 3d electrons. From the perspective of the intrinsic energy of the crystal, the competition between magnetic energy and anisotropy becomes more intense during the SR process, and it is more sensitive to external influence factors. In 2004, Kimel *et al.* reported the inverse Faraday effect and thermal effect of short laser pulses induced by ultrafast spin reversal in $TmFeO_3$ single crystal.[2] The magnetic field induced gigantic magnetoelectric and ferroelectric phenomena in $DyFeO_3$ have also been studied.[15] In addition, terahertz time-domain spectroscopy has been used to describe the SR of $ErFeO_3$, $YFeO_3$,

*Project supported by the National Natural Science Foundation of China (Grant Nos. 12074242 and 51862032), the Ministry of Science and Higher Education of Russia (theme "Spin" No. AAAA-A-18-118020290104-2), and the Government of the Russian Federation (Grant No. 02.A03.21.0006).

†Corresponding author. E-mail: gaotian@shiep.edu.cn
‡Corresponding author. E-mail: sxcao@shu.edu.cn

© 2021 Chinese Physical Society and IOP Publishing Ltd

and $NdFeO_3$ single crystals.[16–18] Temperature induced SR transitions in $SmFeO_3$, $TbFeO_3$, and $Ho_{0.5}Pr_{0.5}FeO_3$ single crystals were detailedly studied.[8,19,20] The investigation of physical mechanism of SR transition in rare-earth orthoferrites can provide a deeper understanding of the the behavior of the 4f and 3d electrons. Besides, multiple magnetic transitions study may help to find new multiferroic and other spintronic materials.

In this work, magnetocrystalline anisotropy and dynamic spin reorientation of half-doped $Nd_{0.5}Pr_{0.5}FeO_3$ single crystal were detailedly studied. The anisotropic magnetic interactions and multiple magnetic phase transitions reflect the complex magnetic structure. The magnetic phase diagram of $Nd_{0.5}Pr_{0.5}FeO_3$ single crystal was finally obtained.

2. Experimental details

The $Nd_{0.5}Pr_{0.5}FeO_3$ single crystals were grown by the optical floating-zone furance (FZ-T-10000-H-VI-P-SH, Crystal System Inc). The preparation process has been described in detail in the previous literature.[21] The crystal morphology and compositional homogeneity were verified by x-ray diffraction (XRD). The orientation and quality of the crystal were determined by Laue back-reflection. Measurements of the magnetization as a function of magnetic field and temperature were conducted by using the physical property measurement system (PPMS-9, Quantum Design) with vibrating sample magnetometer option. In zero-field-cooling (ZFC) measurements, the crystal was cooled down to 2 K without external magnetic field, and then an external magnetic field was applied to conduct measurements during the process of heating to 300 K. The magnetic field dependence of magnetization was measured at selected temperatures after ZFC.

3. Results and discussion

The room temperature powder XRD data of $Nd_{0.5}Pr_{0.5}FeO_3$ single crystal were refined by Rietveld method in the FullProf program.[19] As shown in Fig. 1(a), the diffraction patterns demonstrate the single-phase orthorhombic perovskite structure with space group *Pbnm* and no impure phase was detected. The lattice parameters are obtained to be $a = 5.46650$ Å, $b = 5.58270$ Å, and $c = 7.77310$ Å. The spin-lattice interaction dictates the spin configuration and the canted FeO_6 octahedra, as shown in Fig. 1(b) made by the VESTA software. The clear Laue diffraction spots can easily be observed. Both the XRD pattern and Laue photography confirm the high quality of the single crystal, and the cutting planes are precisely perpendicular to the orthorhombic *a*-, *b*-, and *c*-directions (*Pbnm* setting), respectively.

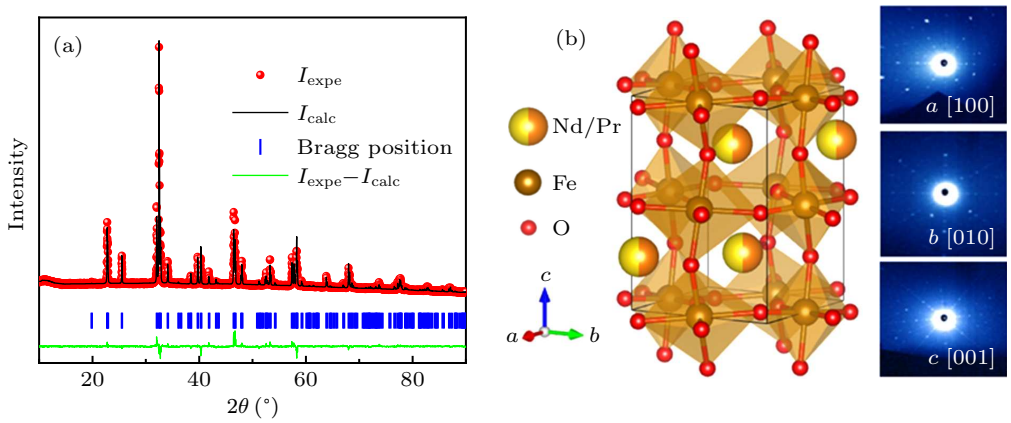


Fig. 1. (a) The rietveld refinement of the powder XRD patterns for $Nd_{0.5}Pr_{0.5}FeO_3$. It shows the experimental, calculated, and difference intensities along with the Bragg positions. (b) The simulated crystallography structure and the Laue photographs along the *a*-, *b*-, and *c*-directions of the $Nd_{0.5}Pr_{0.5}FeO_3$ single crystal.

Figure 2 displays the temperature dependence of magnetization measured with an applied magnetic field $H = 0.01$ T along *a*-, *b*-, and *c*-directions of the $Nd_{0.5}Pr_{0.5}FeO_3$ single crystal. The visible magnetic anisotropy illustrates the complex magnetic interactions. As the temperature goes down from 300 K to 2 K, the sample shifts from a Γ_4 phase to a Γ_2 phase through a SR transition. To determine the phase transition parameters, we evaluated the derivations of the magnetization data at $H = 0.01$ T along *a*- and *c*-directions of the $Nd_{0.5}Pr_{0.5}FeO_3$ single crystal, the plotted curves are shown in Fig. 3. The sample undergoes the SR transition in the temperature window from 45 K to 66 K as marked by green dotted lines. Above $\sim$ 66 K, the sample shows the spin characteristics of Γ_4 phase. That is, it possesses FM moments at *c*-direction, G- and A-type AFM properties at *a*- and *b*-direction, respectively. Similar phenomena have been observed in the $NdFeO_3$ and $PrFeO_3$ orthoferrites.[12,13] Once a temperature below 45 K is achieved, the Fe^{3+} spins shift to a Γ_2 state, where the magnetic structure is changed to FM order, C-type AFM, and G-type AFM order at *a*-, *b*-, and *c*-direction, respectively. In the temperature window of 45–66 K, it exhibits a mixed feature of Γ_4 phase and Γ_2 phase, and illustrates the dynamic transition process of the two phases, which is marked as $\Gamma_{24}(G_{xz}, F_{xz})$ phase. One can see the color area marked as

Γ_2, Γ_{24}, and Γ_4 in Fig. 2. In addition, the maximum value of magnetization at *a*-direction in Γ_2 state is much larger than that of Γ_4 state at *c*-direction. As marked by the blue dotted line, the maximum value of magnetization at *c*-direction in Γ_4 state is ~ 0.76 emu/g, and it changes to $\sim$3.12 emu/g at *a*-direction in Γ_2 state. The maximum value of magnetization in Γ_2 state has increased by $\sim 311\%$ compared to the value in Γ_4 state. Therefore, we reasonably believe that the abnormal increase of magnetization at low temperatures is dominated by a new mechanism of magnetic interaction. It is interesting that the magnetization along the *b*- and *c*-direction in Γ_2 state continuously rises with temperature decreasing to the lowest temperature. As reported in previous literature,[13] the upwarping behavior at low temperatures in $NdFeO_3$ system is related to the increasingly polarization of magnetic rare-earth ions, and the effective moment of the Nd sublattice is antiparallel to that of the Fe sublattice and increases faster when the temperature reaches a compensation point. Furthermore, an enlarged latent plateau around $\sim$ 54 K along *b*-direction is displayed in the figure inset, where the dynamic spin rotation from A-type AFM to C-type AFM state is visibly observed.

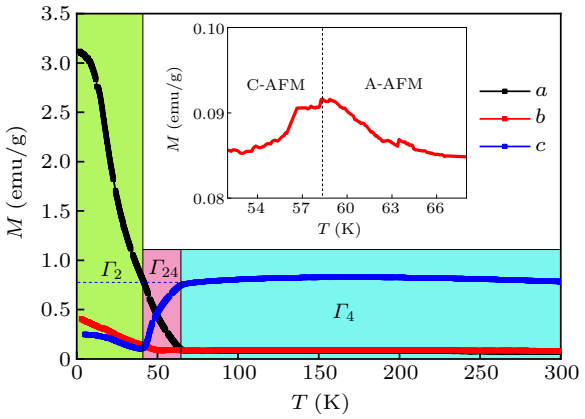


Fig. 2. Temperature dependence of magnetization along the *a*-, *b*- and *c*-direction of $Nd_{0.5}Pr_{0.5}FeO_3$ single crystal, measured in an external field $H = 0.01$ T. Γ_2, Γ_{24} and Γ_4 phases can be distinguished by the shaded areas. The inset is the zoom-in for the spin reorientation transition along the *b*-direction.

The SR transition temperature window is 6.5 K to 10 K for $PrFeO_3$ and 107 K to 170 K for $NdFeO_3$.[12,13] As a mixture of $PrFeO_3$ and $NdFeO_3$, half-doped $Nd_{0.5}Pr_{0.5}FeO_3$ performs the SR transition from Γ_4 to Γ_2 state in the temperature window of 45 K to 66 K, which is exactly the intermediate region between the SR transitions of the two matrixes. The dynamic rotation process of spins is symbolically depicted in the insets of Fig. 3. It is commonly believed that the weak macroscopic FM moment ($\boldsymbol{M}_{Fe} = \boldsymbol{S}_1 + \boldsymbol{S}_2$) is induced by the antisymmetric DM interactions. Here, $\boldsymbol{S}_1$ and $\boldsymbol{S}_2$ are represented as two pairs of spins for Fe^{3+} in the G-type AFM state. While cooling the sample below its Néel temperature, $\boldsymbol{M}_{Fe}$ continues to rotate from the *c*-direction in Γ_4 phase towards the *a*-direction in Γ_2 phase and always stays in the *ac*-plane through the metastable $\Gamma_{24}(G_{xz}, F_{xz})$ phase. As the temperature drops to $\sim$ 17 K, the magnetization is further enhanced and an anomaly occurs at *a*-direction in Fig. 3, which implies a kind of new magnetic interactions and can account for the 311% increase in magnetization as displayed in Fig. 2. The increasing magnetization at $\sim$ 17 K may be linked to the transition from low-spin ($S = 1/2$) to high-spin ($S = 5/2$) state of Fe^{3+}.[22,23] The volume change of Fe^{3+} gives rise to the conflict of atomic Hund rules due to the changed crystal field and results in a further enhancement of the total moment (see the insets of Fig. 3). Another possible source of the unexpected anomaly at $\sim$ 17 K is the R^{3+}–R^{3+} and/or R^{3+}–Fe^{3+} interactions. More in-depth experimental research will be performed in other works.

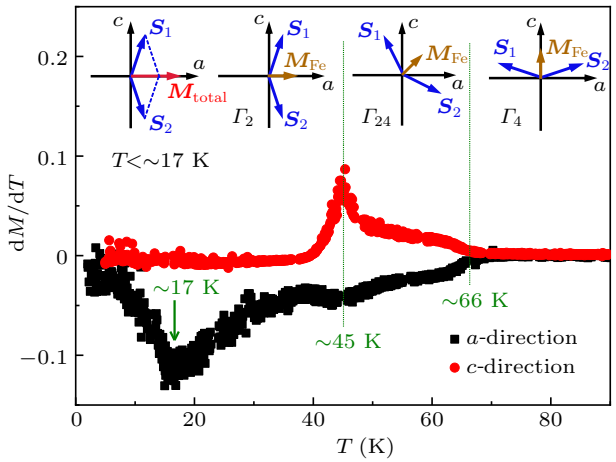


Fig. 3. The calculated derivations of the magnetization data at $H = 0.01$ T along *a*- and *c*-direction of $Nd_{0.5}Pr_{0.5}FeO_3$ single crystal. The temperature window of dynamic spin reorientation is marked with green dotted lines. Insets illustrate the simplified spin configuration for Fe^{3+} and R^{3+}. The two pairs of spins for Fe^{3+} are visualized as $\boldsymbol{S}_1$ and $\boldsymbol{S}_2$ in the G-type AFM state, $\boldsymbol{M}_{Fe}$ represents the resultant FM moment of Fe^{3+}, M_{total} represents the total FM moment of Fe^{3+} and/or R^{3+} at $T <\sim 17$ K.

Figures 4(a)–4(b) show the magnetization curves under different magnitude fields along *a*- and *c*-direction of the single crystal. In order to make the phase transition legible, the coordinate takes in the form of logarithm. It is clear that the magnetic phase transitions are particularly sensitive to the applied magnetic field. In Fig. 4(a), the SR temperature (T_{SR}), marked by the green and red dotted lines, moves to higher temperatures with the increasing magnetic field applied at *a*-direction. Figure 4(b) shows that T_{SR} moves to the lower temperature region under a higher applied field paralleled to *c*-direction. According to the slope change of the magnetization curves, the phase boundaries can be depicted. The corresponding *T*–*H* phase diagrams for $Nd_{0.5}Pr_{0.5}FeO_3$ single crystal are shown in Figs. 4(c) and 4(d). The T_{SR} variation reflects the competition effects of Γ_4 and Γ_2 phases and confirms the inverse effects of magnetic field on magnetic moment at *a*- and *c*-direction. Specifically, the Γ_4 state will be stabilized along *c*-direction by the magnetic field, so the rotation of moments towards basal-plane will be transferred to a lower temperature, resulting in a decrease of T_{SR}. While the rising magnetic field

is applied parallelly to a-direction, it will accelerate the rotation process of moments to a-direction, which yields the increase of T_{SR}. Furthermore, one can see that the T_{SR} along a-direction is evidently higher than that along c-direction under the identical conditions, which is owing to an asynchronous characteristic of the $M(T)$ curves.[24]

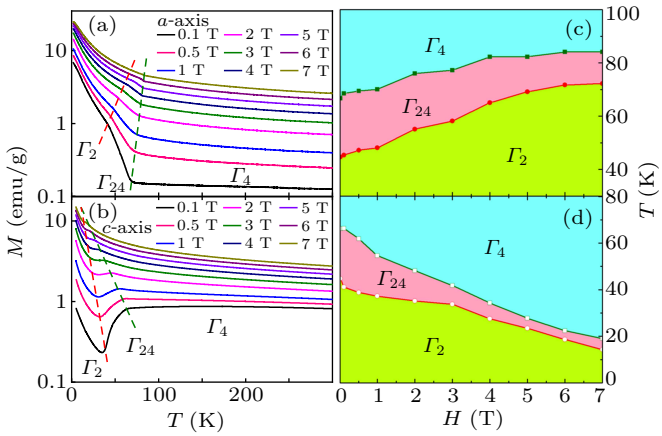


Fig. 4. (a)–(b) Temperature dependence of magnetization at various magnetic field along the a- and c-direction of $Nd_{0.5}Pr_{0.5}FeO_3$ single crystal. Γ_2, Γ_{24} and Γ_4 phases are separated by green and red dotted lines, respectively. (c)–(d) The corresponding phase diagrams for $Nd_{0.5}Pr_{0.5}FeO_3$ single crystal. The phase boundaries are ascertained according to the slope change of the magnetization curves.

The isothermal magnetization loops are characterized to certify the nature of the magnetic state, selected results are shown in Figs. 5(a) and 5(b). In accord with the $M(T)$ data in Figs. 2 and 4, the S-shaped hysteresis loops at a- and c-direction show weak FM features because of the multiple magnetic phase transitions of Fe^{3+} and/or R^{3+}, and the unsaturated magnetization is a typical characteristic of AFM state. The FM moment along the direction of the c-axis at high temperatures ($T \geq 100$ K) is attributed to the canted magnetic moment of Fe^{3+}, which rotates in the direction of the a-axis when the temperature drops below 40 K. In addition, one can see the residual magnetization at 10 K in Fig. 5(a) is much larger than the values in Fig. 5(b). This is due to the occurrence of a new FM phase at ~ 17 K as discussed above. The insets of Fig. 5 are enlargements of the magnetization curves at low magnetic fields, where we can read the coercivity and residual magnetization clearly. In the inset of Fig. 5(a), the coercivity is observed to be zero at $T < 60$ K. From 60 K to up, the coercive force gradually increases. At 300 K, the square shape hysteresis loop with a coercivity of ~ 0.08 T is detected. The coercivity above the SR transition temperature is higher than that below it, which illustrates the stronger anisotropy in the Γ_4 state. Therefore, the magnetic excitation is closely related to the external temperature and applied magnetic field.

To further represent the nature of phase transitions for $Nd_{0.5}Pr_{0.5}FeO_3$ single crystal, we calculated the arrott plots by the isothermal magnetization data, as displayed in Figs. 5(c) and 5(d). The vertical coordinates are shown in logarithmic form for clear. The typical S-shape and the negative slope around ~ 60 K imply a phase transition of first-order, which is believed to be related to the SR transition. By applying an external magnetic field, the temperature of the first-order phase transition in the direction of a-axis moves to the higher temperatures, while that in the direction of c-axis gradually moves to the lower temperatures. Above T_{SR}, the crystal is in the Γ_4 state with the resultant FM vector pointing along the c-direction of the crystal, and the phase transition of first-order is stimulated by a magnetic field along a-direction. While the magnetic field is applied along c-direction, there is no phase transition except that the magnetization is enhanced.

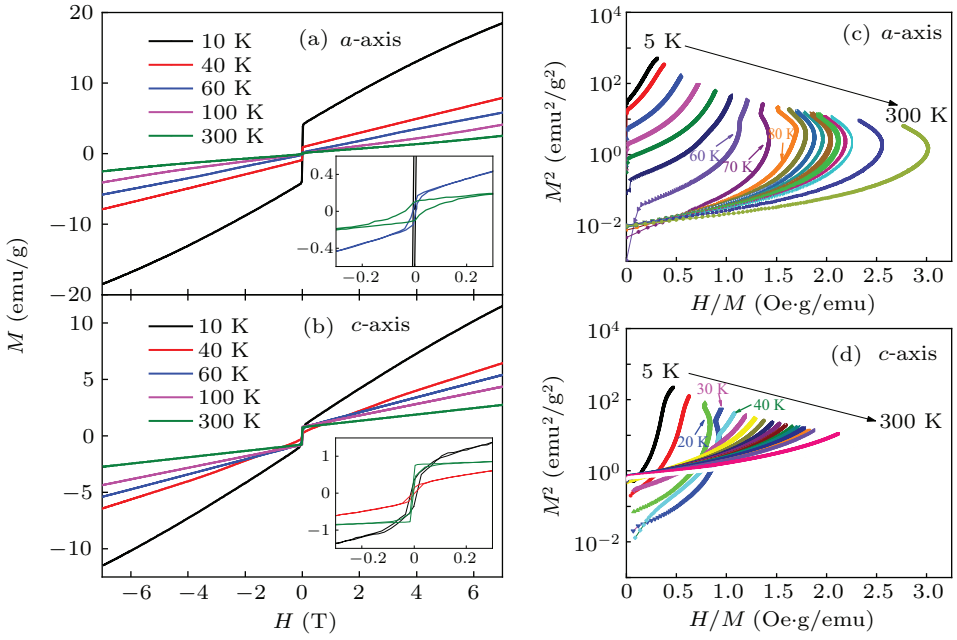


Fig. 5. (a)–(b) Isothermal magnetization hysteresis loops up to 7 T were measured at various temperatures along the a- and c-direction of the $Nd_{0.5}Pr_{0.5}FeO_3$ single crystal. Figure insets are the enlarged curves in the low magnetic fields region. (c) and (d) show the corresponding arrott plots.

4. Conclusion

The excellent quality single crystals of half-doped $Nd_{0.5}Pr_{0.5}FeO_3$ have been successfully grown by using the optical floating zone furnace. The crystal structure was characterized by XRD pattern and Laue back-reflection. The magnetic anisotropy and multiple phase transitions were detected by PPMS-9T under various temperatures and magnetic fields. Below 300 K, the weak FM moment is caused by the famous DM interactions due to the distortion of FeO_6 octahedra, which rotates from the *c*-direction to the *a*-direction of the single crystal (*Pbnm* setting) in the temperature window from 66 K to 45 K. The dynamic SR transition Γ is verified to be first-order by arrott plots in various magnetic fields.

Acknowledgments

The authors thank Dr. Yiming Cao (Qujing Normal University) for the valuable discussion on crystal structure.

The data that support the findings of this study are available from the corresponding author upon reasonable request.

References

[1] Kimel A V, Kirilyuk A, Tsvetkov A, Pisarev R V and Rasing T 2004 *Nature* **429** 850
[2] Wu H L, Cao S X, Liu M, Cao Y M, Kang B J, Zhang J C and Ren W 2014 *Phys. Rev. B* **90** 144415
[3] Leiner J C, Kim T, Park K, Oh J, Perring T G, Walker H C, Xu X, Wang Y, Cheong S W and Park J G 2018 *Phys. Rev. B* **98** 134412
[4] Hoedl M F, Gryaznov D, Merkle R, Kotomin E A and Maier J 2020 *J. Phys. Chem. C* **124** 11780
[5] Mir F A, Sharma S K and Kumar R 2014 *Chin. Phys. B* **23** 048101
[6] Eibschütz M, Shtrikman S and Treves D 1967 *Phys. Rev. B* **156** 562
[7] Yuan N, Li R B, Yu Y S, Feng Z J, Kang B J, Zhuo S Y, Ge J Y, Zhang J C and Cao S X 2018 *Front. Phys.* **14** 13502
[8] Cao Y M, Xiang M L, Zhao W Y, Wang G H, Feng Z J, Kang B J, Stroppa A, Zhang J C, Ren W and Cao S X 2016 *J. Appl. Phys.* **119** 063904
[9] Waber M C, Guennou M, Hong J Z, Iniguez J, Vilarinho R, Almedia A, Agostinho M J and Kreisel J 2016 *Phys. Rev. B* **94** 214103
[10] Li Q Y, Zhao D and Li Z D 2021 *Chin. Phys. B* **30** 017504
[11] Cao S X, Chen L, Zhao W Y, Xu K, Wang G h, Yang Y L, Kang B J, Zhao H J, Chen P, Stroppa A, Zheng R K, Zhang J C, Ren W, Íñiguez J and Bellaiche L 2016 *Sci. Rep.* **6** 37529
[12] Yuan S J, Ren W, Hong F, Wang Y B, Zhang J C, Bellaiche L, Cao S X and Cao G 2013 *Phys. Rev. B* **87** 184405
[13] Li E Y, Feng Z, Kang B J, Zhang J C, Ren W and Cao S X 2019 *J. Alloy. Compd.* **811** 152043
[14] Shen H, Cheng Z X, Hong F, Xu J Y and Yuan S J 2013 *Appl. Phys. Lett.* **103** 192404
[15] Tokunaga Y, Iguchi S, Arima T and Tokura Y 2008 *Phys. Rev. Lett.* **101** 097205
[16] Mikhaylovskiy R V, Hendry E, Kruglyak V V, Pisarev R V, Rasing T and Kimel A V 2014 *Phys. Rev. B* **90** 184405
[17] Zhou R Z, Jin Z M, Li G F, Ma G H, Cheng Z X and Wang X L 2012 *Appl. Phys. Lett.* **100** 061102
[18] Jiang J J, Jin Z M, Song G B, Lin X, Ma G H and Cao S X 2013 *Appl. Phys. Lett.* **103** 062403
[19] Cao S X, Zhao H Z, Kang B J, Zhang J C and Ren W 2014 *Sci. Rep.* **4** 5960
[20] Wang G H, Zhao W Y, Cao Y M, Kang B J, Zhang J C, Ren W and Cao S X 2016 *J. Alloy. Compd.* **674** 300
[21] Chen L, Li T W, Cao S X, Yuan S J and Hong F 2012 *J. Appl. Phys.* **111** 103905
[22] Gütlich P, Hauser A and Spiering H 1994 *Angew. Chem.* **33** 2024
[23] Zhang W and Huang J 2016 *Chin. Phys. B* **25** 057103
[24] Cao Y M, Xu K, Li Z, Zhang Y L, He X J, Kang Y R, Sun W, Gao T, Qian Z, Liu C Q, Ye M F and Jing C 2019 *J. Magn. Magn. Mater.* **487** 165315